Analysis of laser-induced contamination at 515 nm in the sub-ps/MHz regime

Georges Gebrayel El Reaidy, Laurent Gallais

Analysis of Laser-Induced Contamination at 515 nm in the sub-ps/MHz regime.

Georges Gebrayel El Reaidy,[†] Laurent Gallais[*]
Aix Marseille Univ, CNRS, Centrale Marseille, Institut Fresnel, France

Abstract. We study Laser-Induced Contamination (LIC) as a potential cause of optical losses and Laser-Induced Damage (LID) of optical components for ultrashort pulse lasers with high average power in the MHz regime. Our work is conducted on dichroic mirrors designed for maximum reflection at 515nm operated in ambient air. Based on the development of an experimental set-up for real time monitoring of LIC and accelerated test protocols, we have conducted a parametric study on LIC development and studied its growth dynamics and morphology. We show that LIC is a main limitation of short wavelength high average power fs/ps lasers, with the formation of nanometric highly absorbing layers of carbonate compounds on the laser footprint, with evidence of thermal effects. It is also found that the last layer of the stack, at the interface between air and coating stack, is critical in the LIC growth which can open some perspectives for limitation of this effect.

Keywords: laser damage, laser-induced contamination, ultrashort pulse lasers.

*****E-mail: laurent.gallais@fresnel.fr

1 Introduction

In the field of laser processing, marking and drilling require increasingly precise high quality process so that the needs for higher power and shorter wavelength femtosecond lasers are increasing very fast. For instance, the progress in display technologies stimulates the development of a new generation of lasers with shorter pulses for better processing.[1,2] Diode-pumped femtosecond lasers with frequency converted output are excellent candidates to fulfil this need, thanks to ultra-short pulse durations and high photon energies, but fundamental physical effects limit the lifetime of optical components. The critical components in these laser systems are mainly the optical interference coatings used as mirrors, dichroic filters, or antireflectors on crystals.[3] There are physical limitations to the power handling capabilities of such components. At high

[†] Now at Aix Marseille Univ, CNRS, LP3, France

intensity, non-linear ionization processes can cause a strong coupling of the laser beam energy in the material leading to the onset of catastrophic damage.[4] With respect to such physical mechanisms, there is a clear intrinsic limitation and a ranking of the laser damage resistance of materials based on their bandgap.[5,6] With some optimized designs taking into account these intrinsic properties of the materials it is possible, by avoiding intensity peaks in materials with low Lased-Induced Damage Threshold (LIDT), to enhance significantly the laser damage resistance of multilayer stacks.[7–9] However, in the case of high repetition rate lasers other complex processes can lead to the reduction of the laser damage resistance with the number of pulses: generation of electronic defects in the materials that eases the ionization process,[10,11] heat accumulation leading to stress-build-up and potential failure,[12,13] damage growth initiated by localized defects.[14–17] At this point only laser damage tests in conditions as close as possible to the applications can be used to predict the lifetime of the components and their power handling capabilities. However, even if the components have proven high LIDT, their long term reliability can be unsatisfactory even if they are operated under this limit. A particularly detrimental effect is the interaction between the laser beam, the volatiles compounds in the ambient atmosphere, and the optical surface, that can trigger the formation of nanometric highly absorbing layers. This unwanted deposition process, referred as Laser-Induced Contamination (LIC), can be responsible for an accelerated transmission loss and finally non-reversible laser damage of the optical components, possibly causing laser failure.[18–22] This effect is critical for the industrial applications, and it has mainly been studied in the context of space applications: several past spaceflight missions using ns UV lasers proved to be short-lived and unreliable due to this effect, which has initiated an active field of research between space and laser communities.[23–30] LIC effects in the fs/ps regime have not been reported in the opened literature up to now but our investigations on laser components have led us to the

conclusion that these effects are also particularly detrimental in this regime and can be a main limitation of short wavelength high average power fs/ps lasers (Figure 1).

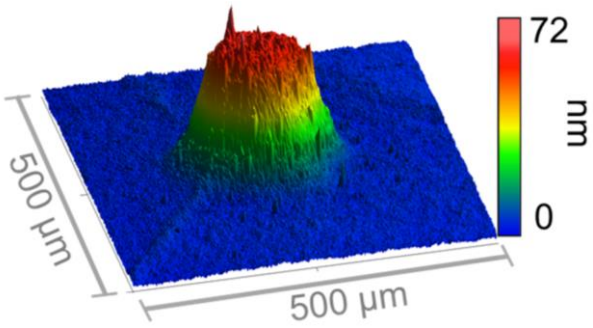

Figure 1: A LIC deposit on a dielectric mirror exposed to 700 fs/ 515 nm/ 30 MHz laser with 35 W of mean power and 130 µm beam diameter (surface topography measured using White Light Interferometry).

Therefore, in this work we would like to investigate these effects with a first report on the topic. Our motivation is that in order to improve lifetime of optical components it is firstly required to precisely measure their degradation as a function of laser parameters (operating time, mean power, repetition rate, etc…) in order to quantify the LIC process. Secondly it is also necessary to perform accelerated tests since the typical specification of lasers is few 10000 h and it is not convenient to conduct laboratory studies with such long durations. Eventually when conclusive tests have been demonstrated based on their representativeness compared to real laser operation on thousands of hours, an investigation of different samples can be conducted in order to understand LIC formation and identify the best candidates for the application.

For that purpose, we will firstly describe in this paper the experimental system that has been implemented to perform representative tests in the sub-ps MHz regime at 515 nm, based on an industrial laser source. We will then report our results on the observation of LIC formation in different irradiation conditions, associated to morphological and optical characterization of the

LIC deposit. Eventually we will discuss on the LIC formation dynamic and associated thermal effects based on *in situ* measurements.

2 Experiments

There exists different experimental set-up in the scientific community to conduct laser-damage tests relevant to the study of LIC effect. Some of them were developed for LIC tests for space optics,[22,24–26,31–33] with particular emphasis to exposure to nanosecond UV lasers. In this case, space conditions are simulated with a high vacuum chamber and the contamination process is controlled by introducing a specific contaminant into the chamber. To investigate damage formation, *in situ* diagnostics can be installed to monitor the sample inside the chamber during irradiation. Complementary on-line detection approaches such as measurement of transmission loss[21,22] and Laser-Induced Fluorescence[34] were proved to be the most efficient and useful techniques to study the LIC effect. Other studies were also conducted in the context of high power laser facilities for fusion experiments, also dealing with molecular contamination under exposure to nanosecond UV lasers.[35–38] In that case, the repetition rate is very low and the number of laser shots is very limited. *Ex situ* diagnostics such as Nomarski Microscopy, Confocal Fluorescence Microscopy (CLSM), White Light Interferometry (WLIM), Atomic Force Microscopy (AFM) are the most relevant tools of investigation. Taking benefit of this experience we have built a laser damage testing bench allowing *in situ* observation of the sample with real time measurements of transmission losses. Because the laser sources of interest in our study operate at ambient pressure, the system was designed to operate in ambient air environment. Additional capabilities that we will describe below allow a more complete characterization of the LIC deposits.

2.1 Experimental set-up

The experiment is based on a high power industrial laser source that delivers 700 fs pulses at 515 nm with a frequency of 3.3 MHz. The mean power is 35 W, corresponding to an energy per pulse of approximately 10 µJ. Unless specified otherwise in the text, the laser source has always been used at these settings. The beam is linearly polarized and is characterized by a Gaussian spatial distribution with a $M^2 \leq 1.3$. After passing on a set of dielectric mirrors, as described on Figure 2, the beam is focused on the sample with a fused silica plano-convex lens (200 mm focal length). The position of the lens can be adjusted with a motorized linear stage in order to adjust the beam size on the sample. This enables us to adjust the incident fluence while using the full power of the laser source, avoiding the use of a waveplate / polarizer combination. After being transmitted or reflected, depending on the type of tested sample, the beam power is monitored with a calorimeter in order to detect potential drops in transmission of reflection that would be related to contamination or damage.

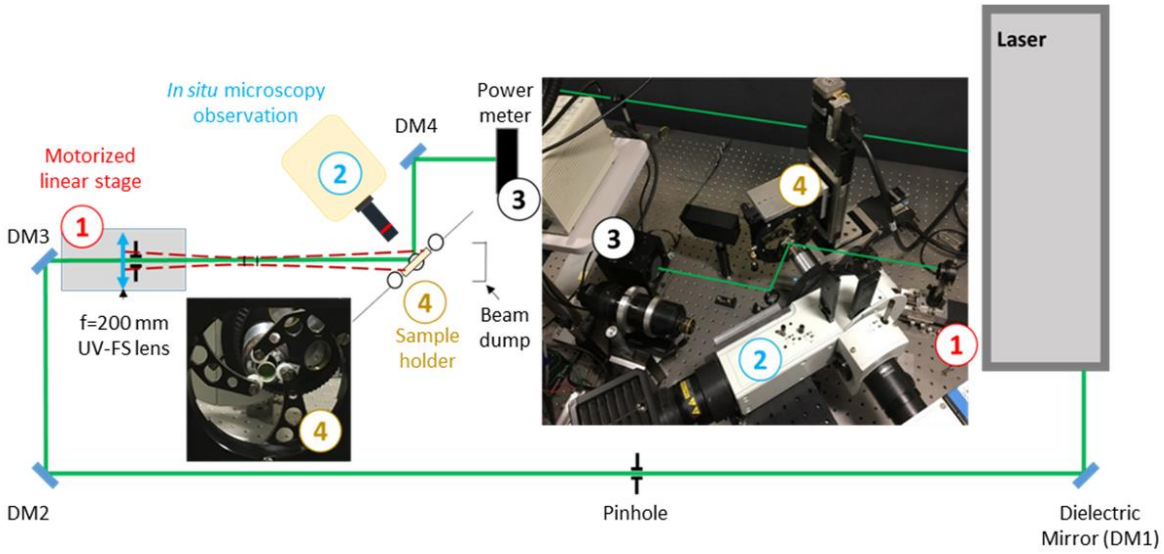

Figure 2: The experimental configuration, described here for the tests of High-Reflectors with 45 degrees of incidence. The inserted image on the right is a close view of the sample area, with (1) the focusing lens, (2) the microscope, (3) the calorimeter and (4) the sample holder. These different elements are also numbered in the schematic. The inserted image on the left is a close view of one sample in the holder, with the microscope beneath it.

The sample was positioned on a motorized holder, with adjustable angle of incidence: experiments have been performed at 45° for High-Reflectors (HR) and close to normal incidence for Anti-Reflective (AR) coatings (not reported here). The front face of the sample was observed at normal incidence via an optical microscope equipped with long working distance objectives and a CMOS Camera. Filters were inserted between the objective and the tube lens to block the scattering from the intense green light and a broadband halogen lamp was used as the illumination source. Other observation modes, particularly with a thermal camera, will be described in next sections.

2.2 Beam characterization

The beam profile has been characterized with a CCD sensor placed in the sample plane. The measurements were conducted in a low power mode operation of the laser source and with a set of filters in the beam path. Measurements for different positions of the focus lens are reported on Figure 3. The characterization of the beam profile is reported as the effective surface of the beam, as defined in the ISO standard[39] in order to obtain the fluence, or as the beam diameter with a Gaussian beam fit of the profile. At the focal position of the lens, the minimum spot diameter was about 35 µm, but we have worked after the focal plane, with diameters in the range of 80 to 550 µm.

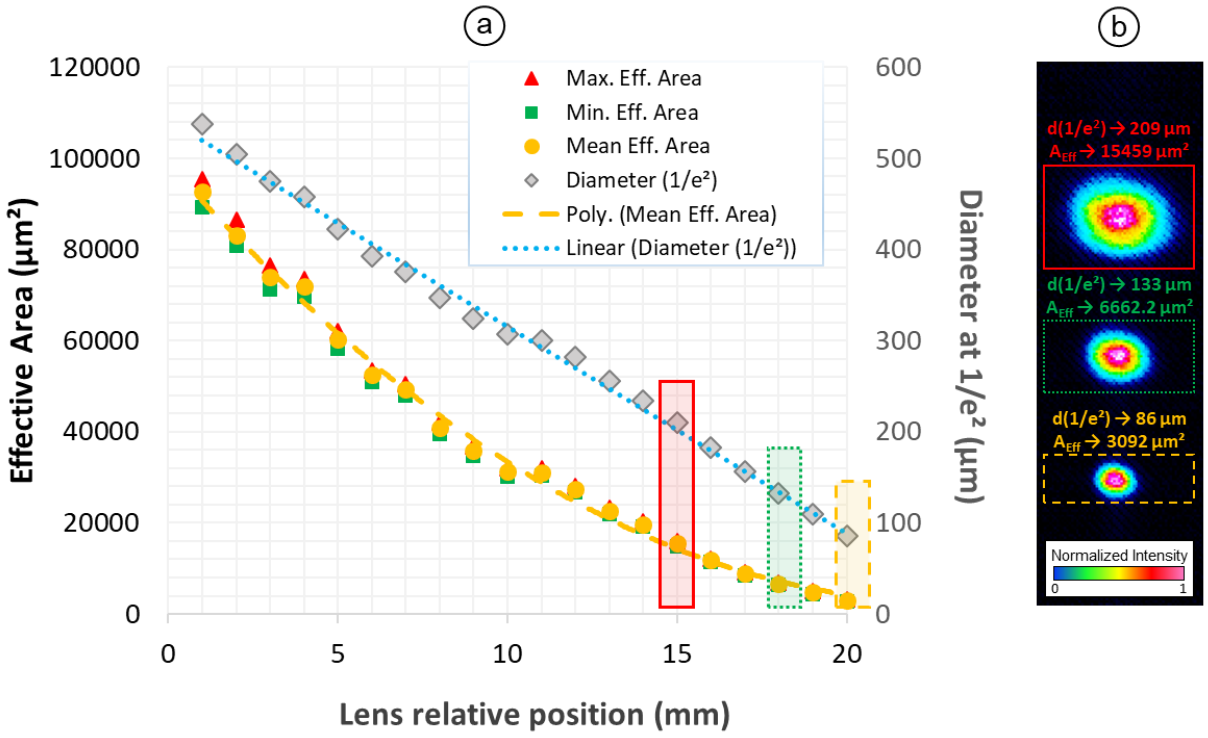

Figure 3: (a) Caustics of the focused laser beam by a plano-convex fused silica lens (f = 200 mm) measured via a beam profiler system (WinCamD-UHR). (b) Spatial beam profile when moving the focusing lens in different positions (All spatial beam profiles use similar scales).

2.3 Test procedures

Tests were conducted by irradiating the sample of interest for different amount of time, typically few hours up to 115 hours at 3.3 MHz and 35 W of incident power. The laser shot sequence was stopped either if damage growth is detected with the online microscope (Figure 4-a), in order to avoid contamination by debris on the surface, or at the end of the defined irradiation time for further *ex situ* analysis. The distance between each tested site was larger than 1 mm.

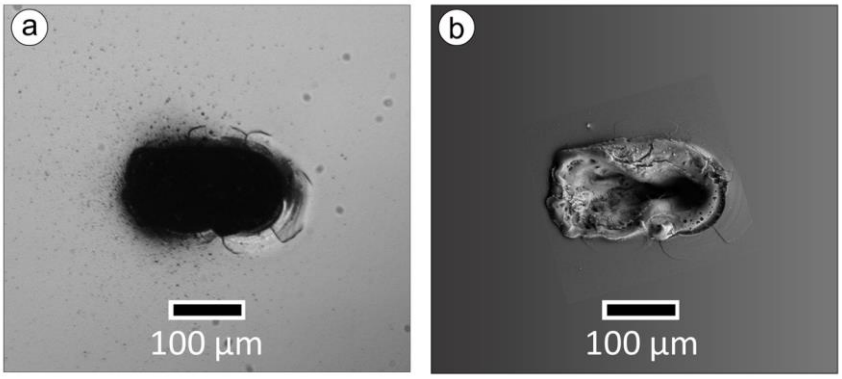

Figure 4: Laser damage observed via (a) online microscopy and (b) Scanning Electron Microscopy on a HR mirror after 23 hours of laser exposure at 515 nm, 700 fs, 3.3 MHz, 35 W focused down to 86 µm diameter on the surface. Both figures use similar lateral scales.

2.4 Characterization of LIC deposits

Analysis of surface modification (LIC deposit) and subsequent performance degradation are done *in situ* by Nomarski microscopy and transmission measurements (Figure 5).

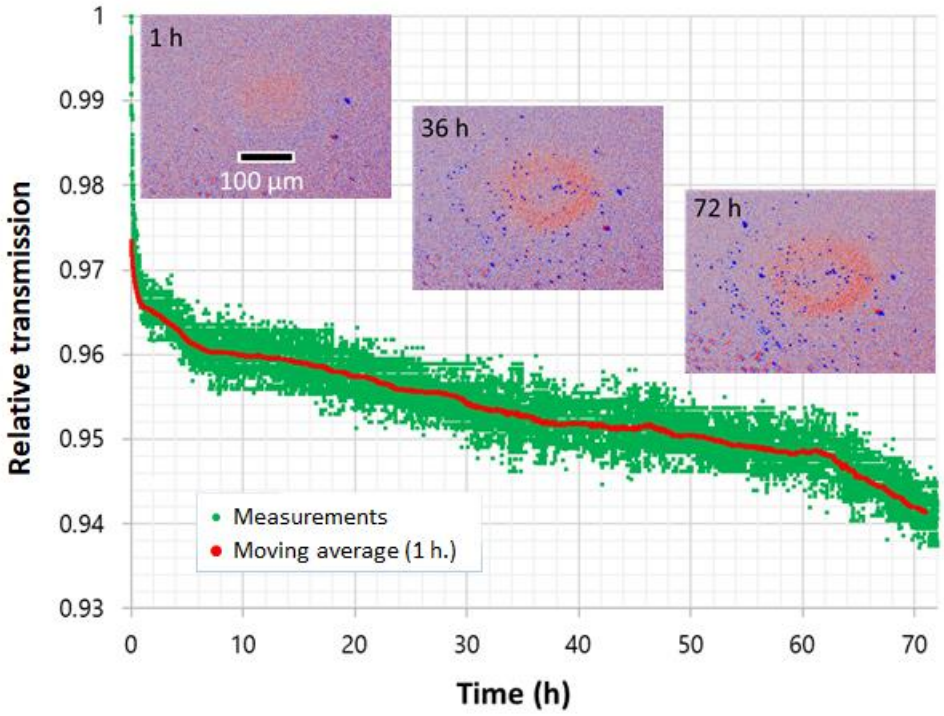

Figure 5: *In situ* images showing the dynamics of LIC deposit formation on the surface of a HR mirror associated to transmission measurement. Test conditions: 72 hours of laser exposure at 515 nm, 700 fs, 3.3 MHz and 35 W focused down to 157 µm diameter on the surface.

Multiple *ex situ* techniques were used to characterize LIC deposits. Optical microscopy using the Differential Interference Contrast (DIC) mode and/or Scanning Electron Microscopy (Figure 4(b)) for quick observations, the WLIM (Zygo NewView 7300), and/or the AFM (Brucker, Dimension Edge) to characterize the physical thickness, a confocal microscope (Leica DM 5500) for *ex-situ* fluorescence measurements and finally a quantitative phase microscope that allows the imaging of both the intensity and the phase of transmitted light. This last microscope is equipped with 10 different monochromatic sources that cover the visible region (470 to 780 nm).[40] Figure 6 shows examples of measurements for each characterization method.

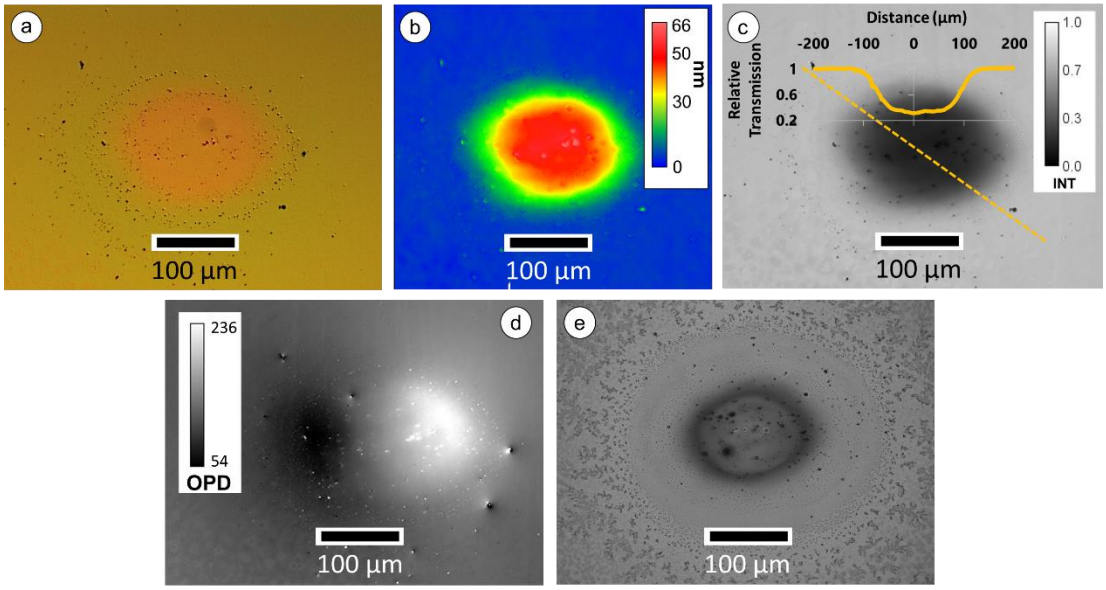

Figure 6: (a) LIC deposit footprint (Same test shown in Figure 5) inspected via different *ex situ* diagnostics: (a) Optical Microscopy, (b) White Light Interferometry, (c) Transmittance and (d) Optical Path Difference (OPD) images for 590 nm wavelength light, (e) Confocal Microscopy (excitation at 488 nm). All figures (a-e) use similar scales.

3 Results and Discussion

In this work we have investigated dichroic mirrors used as separators between the fundamental wavelength (1030 nm) and the second-harmonic (515 nm). The samples were commercial components, with coatings deposited on 12.5 mm diameter UV Fused Silica substrates. The stacks are made of SiO_2 for the low index material and either Al_2O_3 or HfO_2 for the high-index material. Designs are unfortunately not available but we will disclose the last layer upon availability since this last layer has a critical effect on LIC. Such components are used after the non-linear crystal and are usually exposed to the highest green power. The 515 nm is reflected at 45° of incidence, and the 1030 nm is transmitted. In our tests we have only investigated the effect of the green reflected light. Possible effects of simultaneous wavelength exposure were not investigated but some coupling mechanisms could exist as it has been reported in other conditions.[41,42]

3.1 LIC formation under accelerated tests

Laser-Induced Contamination is a deleterious effect that can develop with a very slow dynamic such that in some conditions it can takes thousands of hours to observe significant effects, as observed for instance on space mission instruments.[43,44] In order to conduct tests in a laboratory environment in reasonable conditions it is necessary to perform accelerated tests, i.e. tests with frequencies and fluence higher than in nominal conditions. It is therefore important to ensure that in such test conditions the effects can be comparable to the ones in nominal conditions. This has been done in our work with qualitative comparisons of the laser-induced deposits generated in different conditions.

To optimize the test conditions, we have set the repetition rate of our laser source up to its maximum (3.3 MHz) and the power to its maximum (35 W). Then the beam size has been adjusted to control the fluence. In such conditions it has been possible to observe the LIC effect occurring in few hours' duration, representative of effects observed on few hundreds of hours with lower fluences (Figure 7).

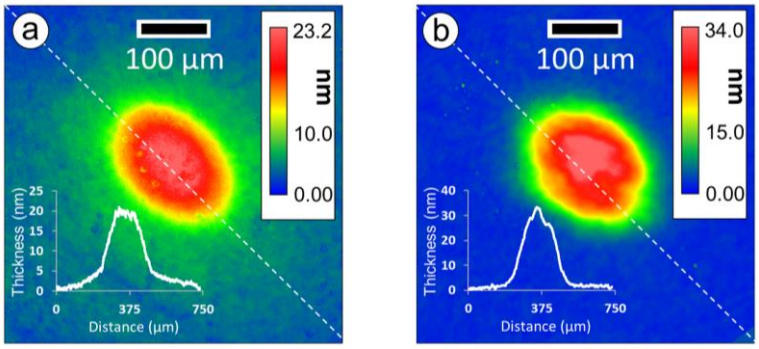

Figure 7: (a) Results of the 515-nm irradiation on a dichroic mirror during 300 hours with d_{1/e^2} = 200 µm, 700 fs, 2 MHz and 28 W (b) Results of irradiation using the same dichroic mirror during 18 hours with d_{1/e^2} = 210 µm, 700 fs, 3.3 MHz and 35 W.

We found that investigations could be conducted in the range between 2 h to 72 h for practical considerations. In such conditions the tests were very repeatable, i.e. LIC deposits have the same thickness and surface for identical irradiation conditions, as shown on Figure 8.

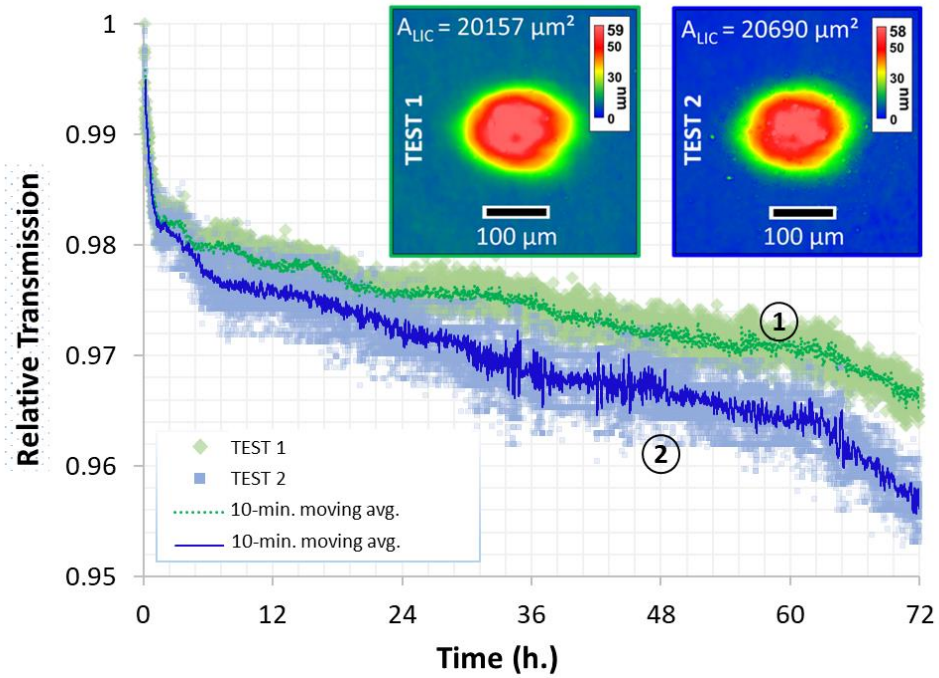

Figure 8: Two different tests performed on a sample under the same conditions. LIC deposits were inspected after each run (WLIM). Test conditions: 72 hours of laser exposure at 515 nm, 700 fs, 3.3 MHz and 35 W focused down to 157 µm diameter on the surface.

For a given irradiation time, the LIC deposit thickness was found to scale linearly with the fluence, as evidence on Figure 9. The scaling coefficient is however strongly dependent on the coating design and manufacturing process, as suggested by the comparison of results obtained on two samples shown on Figure 9. More precisely, the last layer of the stack, at the interface between air and coating stack, was found to be critical. For instance, sample 1 of Figure 9 is an Electron Beam Deposited (EBD) coating with SiO_2 as the last layer, whereas sample 2 is an Ion Beam Sputtering (IBS) deposited coating with SiO_2 also as the last layer. If this result should not be extended to other samples and exposure conditions because only two sets of mirrors were at our disposal for this study, the last layer material and its properties (roughness, porosity, etc…) should be the

subject of deep investigation to mitigate LIC hazard. On this point it was also evidenced in the study of P. Wagner et al.[45] that LIC deposits grow faster on SiO_2 IBS coatings than on EBD coatings, but in very different conditions (vacuum, UV and ns pulses). Recent work suggests also that a design with HfO_2 as the last layer can reduce significantly the growth as compared to SiO_2.[46]

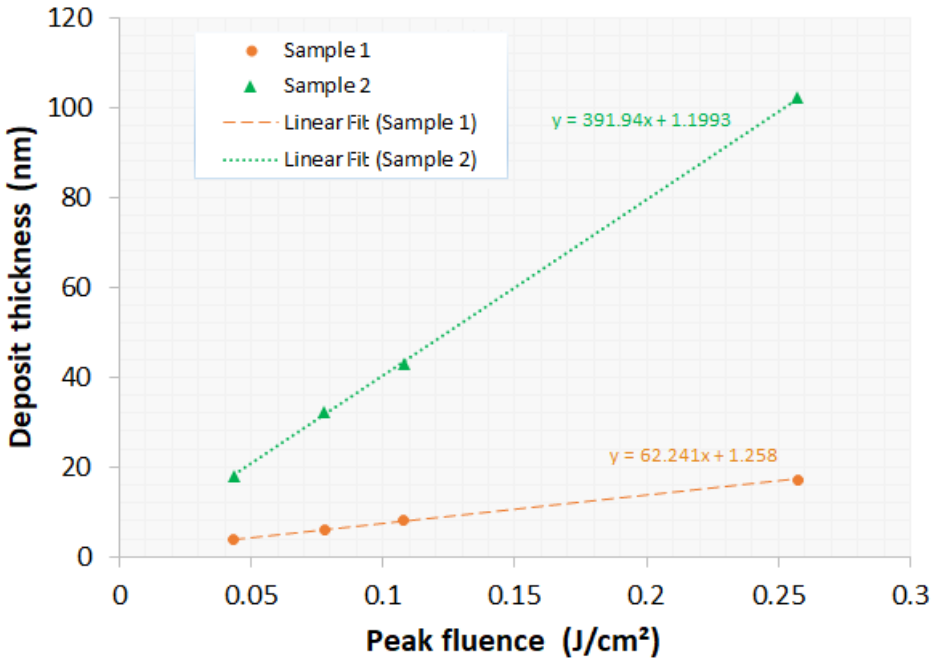

Figure 9: Variation of LIC deposit thickness measured via WLIM, after 2 hours of laser exposure (700 fs, 3.3 MHz, 35 W) with spot sizes in the range 87-210 µm (diameter at 1/e²).

3.2 Dynamics of LIC formation

The LIC deposit formation is a slow evolving process that has a dynamic which is fluence dependent. Figure 10 reports on the *in situ* observation of the formation of a LIC deposit that is characterized by a bump on the center of the laser spot and at later time the formation of small islands in the edge of the exposed area (example Figure 10, 18 h, with ~10 µm islands evidenced on the figure as ”blue dots”). This behavior has been observed in all our tests (see also Figure 5 for 72 h irradiation).

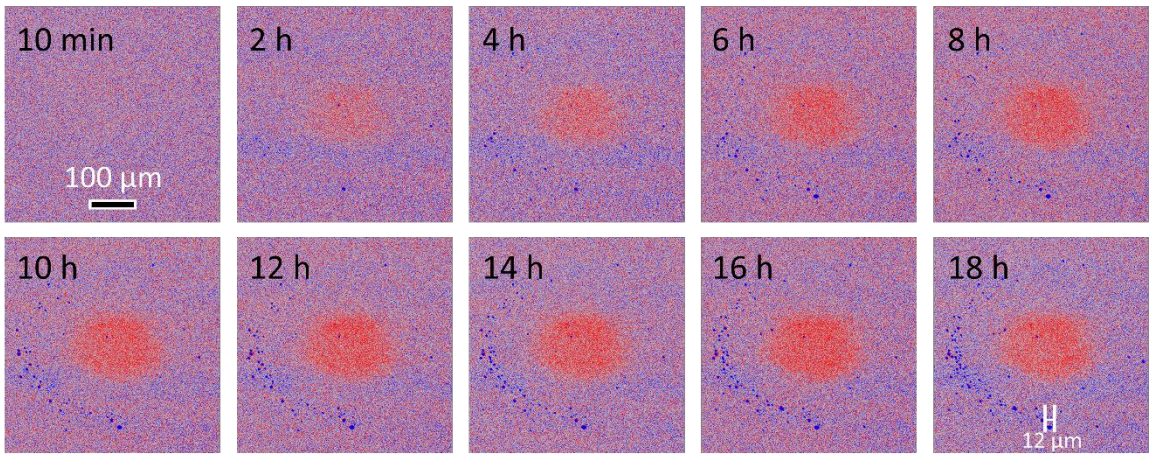

Figure 10: Dynamic of deposit formation on the surface of a HR mirror. Test conditions: 18 hours of laser exposure at 515 nm, 700 fs, 3.3 MHz and 35 W focused down to 210 µm diameter on the surface.

For a given fluence and different exposure times it was found that the LIC deposit thickness saturates at some point and that the morphology of the LIC deposit evolves from a bump to a flat top profile (Figure 11). Evolution of LIC morphologies from "pancake" to "donut" shapes are found in the literature.[47] A lateral growth during the irradiation was also evidenced as shown on the Figure. In fact, this morphology is typical of LIC growth and has been well explained by W. Riede et al.[26] At the beginning of irradiation, a steady growth of the deposit is observed with a pancake-like structure, then a competing process of deposit removal starts at the center of the deposit, i.e. the region of highest laser intensity leading to material removal (because of high absorption of the deposited material). This process then dominates and the "doughnut" structure develops with an increasing central hole. The transition from "pancake" to "doughnut" growth is dependent on laser fluence and in case of very low fluences "pancake" growth can dominate. These processes were described in the UV (355 nm) and more recent studies have shown an even growing importance of LIC in the deep UV (266 nm).[48] In our case the self-limiting vertical growth of LIC

deposit could also be caused by absorption, possibly by two-photon absorption in the deep UV because of the short pulse duration and high intensity.

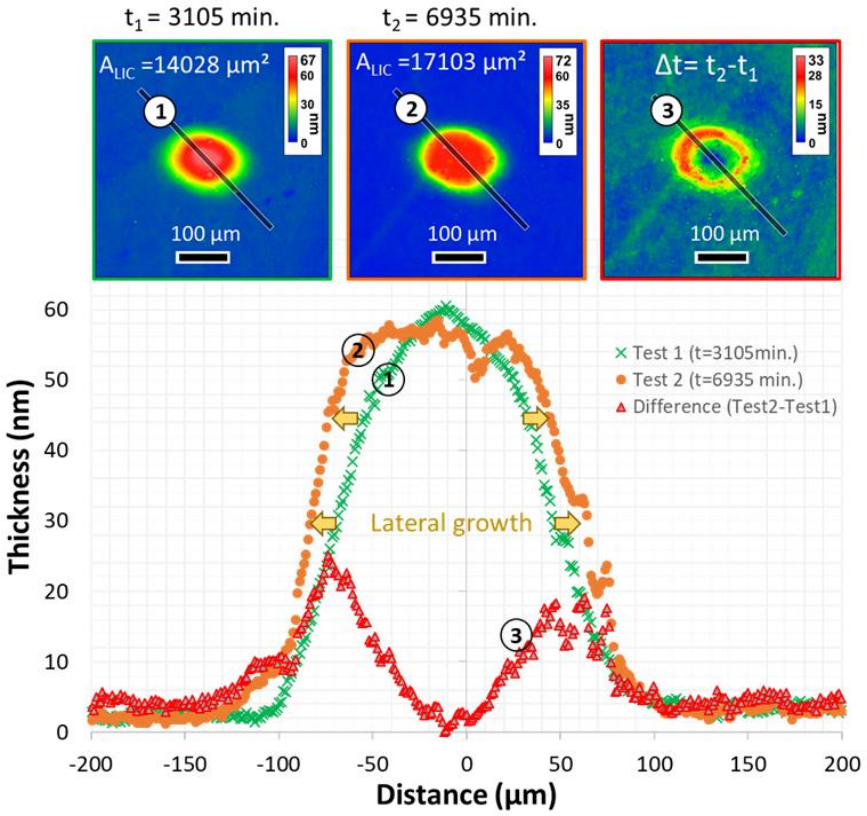

Figure 11: Dynamic of deposit formation. The deposit height was measured via WLIM. The test was performed at a wavelength of 515 nm, a pulse duration of 700 fs, a repetition rate 3.3 MHz and 35 W focused down to 133 µm diameter on the surface.

3.3 Optical properties of LIC deposits.

As shown in the previously reported results, the formation of the LIC deposit is characterized by a degradation of the optical function of the component, a loss of reflectivity of the mirror in our cases (examples on Figure 5 and 8). It is then of interest to study the optical properties of the deposit. If the thickness can be well characterized with AFM or WLIM, access to the optical properties (complex refractive index) of the deposited material requires localized

spectrophotometric or interferometric measurements. A quantitative phase microscopy technique has been applied for that purpose in previous works from our group (the measurement methodology and tools were described in detail in this paper).[30] With this system it is possible to obtain intensity and phase data on the observed object. However, in our case the phase data were not exploitable because of the lack of knowledge on the sample design (refractive index and thickness of each layer of the stack), we will therefore only deal with intensity measurements.

The dichroic mirror coated for high reflectivity (R-99.8%) at 515 nm (AOI = 45°) has been irradiated for 72 hours at 3.3 MHz with a peak power of 35 W, with a result of 60 nm height LIC deposit, as shown on Figure 12 (a). The region of interest was observed under the microscope in transmission mode with illumination using different monochromatic sources (470, 505, 530, 565, 590, 625, 660, 680, 730 and 780 nm). The sample was observed at normal incidence and in such conditions the reflectivity peak of the coating is shifted to longer wavelengths compared to the 515-nm design. Figure 12 (b), (c) and (d) show relative transmission images of the LIC area measured with different wavelengths below the reflection peak (530 nm), at maximum reflection (590 nm) and beyond the reflection peak (625 nm). These measurements show that the relative transmission for different zones depends greatly on the incident wavelength. As shown in Fig 12 (b, c and d), for 530 nm the LIC deposit transmission is higher than 1 (T=1.06), contrariwise for 590 nm the transmission is extremely below 1 (T=0.32) and at 625 nm it is slightly below 1 (T=0.95). These measurements indicate that the LIC deposit behaves like an interference coating on the multilayer stack and that the reflectivity drop observed in the experiments after hours of exposure could be due to interferential effects introduced by the LIC deposit, whereas scattering or absorption could have been suspected as the primary cause. Possibly a combination of absorption and interferential effects could cause the reflectivity drop since carbonaceous

compounds have a high extinction coefficient.[49] Further analysis with samples of known designs is required to explore this point.

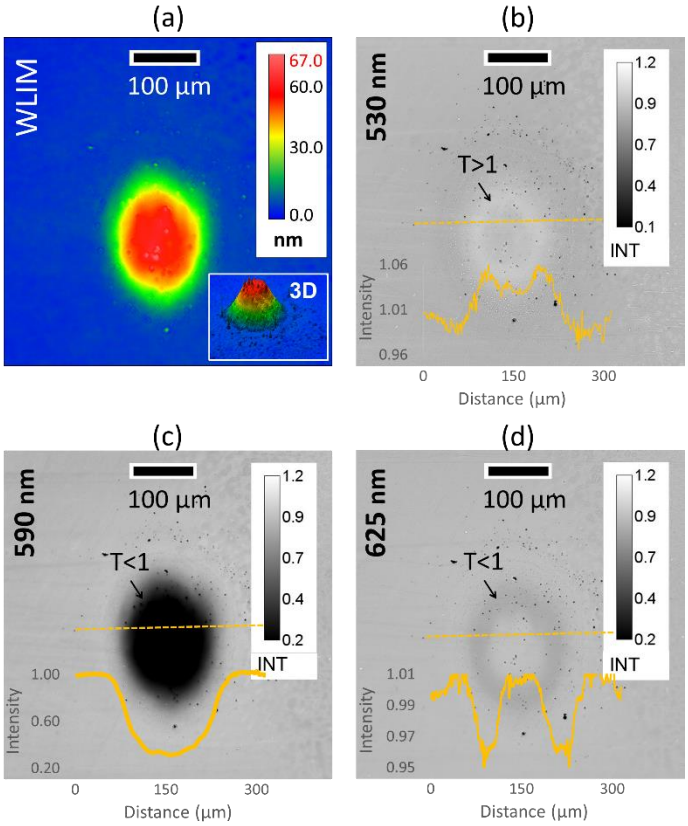

Figure 12: (a) *Ex situ* WLIM of the irradiated site. Relative transmission of the LIC deposit using different monochromatic sources at (b) 530 nm, (c) 590 nm and (d) 625 nm. Test conditions: 72 hours of laser exposure at 515 nm, 700 fs, 3.3 MHz and 35 W focused down to 157 µm diameter on the surface.

3.4 Thermal measurements

To go further in the analysis of LIC, we have investigated the thermal effects related to the growth of the deposit. Indeed, the formation of a contamination layer under the laser spot is associated to absorption of part of the laser power which can lead to local temperature increase. Considering the high repetition rate in our irradiation conditions, the temperature cannot relax back to the ambient temperature between two pulses[50] and the temperature will increase up to a steady state regime where the heat coupled in the deposit by laser absorption is compensated by losses. The surface

temperature increase in such conditions could play an important role in the laser-induced deposition process, the adsorption and sticking coefficient of volatized compounds on surfaces being temperature dependent processes[26] and thermal effects have already been suggested as a possible contribution of LIC.[30]. **Figure 13** shows the lateral expansion of the LIC deposit into regions "far" away from the beam center.

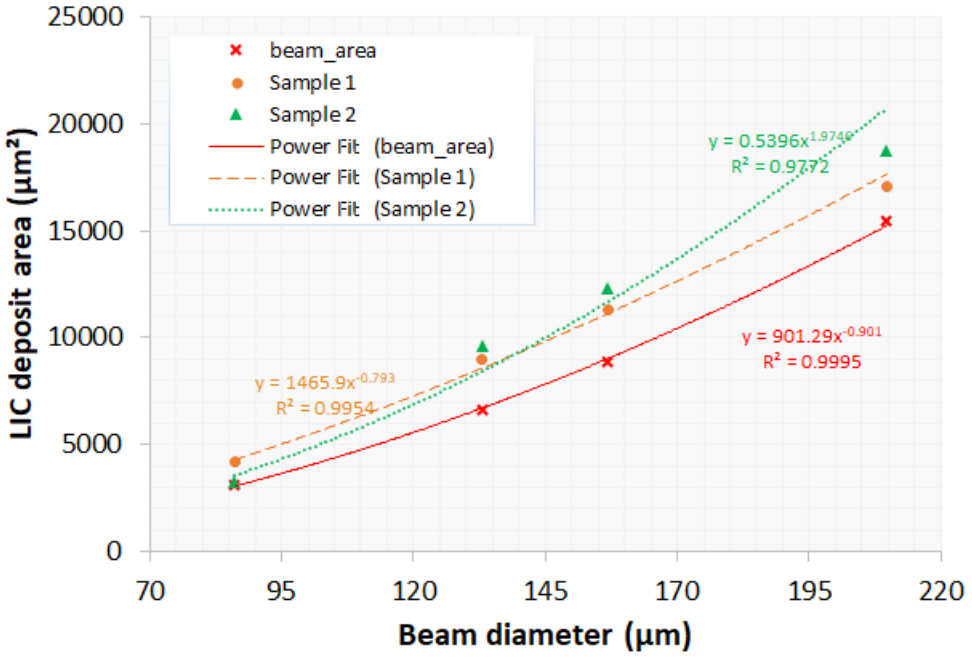

Figure 13: Comparison between LIC deposits area measured via WLIM, after 2 hours of laser exposure (700 fs, 3.3 MHz, 35 W) and the beam area at different spot sizes.

For temperature measurement we have used a thermal camera (OPTRIS PI 640) operating in the LWIR band (8-13 µm) with the emissivity set to 0.85 for the sample under consideration. The spatial resolution was approximately 200 µm in the imaging configuration**, so that for a 500 µm diameter beam, 2 x 2 pixels were imaging the exposed area The integration time of the thermal camera was 8 ms, then each image frame is the result of an average on many laser pulses.** We present **on Figure 14** an example of a measurement with recording of temperature evolution during 7 hours of laser exposure at 3.3 MHz with a peak power of 35 W and a beam

diameter of 550 µm of a mirror with occurrence of LIC. In such conditions the LIC deposit is characterized by a final thickness of 50 nm (characterized after exposure). The thermal measurements indicate a temperature gradient from the center of the irradiated area to the sample sides with a maximum temperature rise of 5.3 °C. We point out that the peak temperature cannot be resolved in our measurement conditions and the temperature rise may therefore be higher. It can be observed that the temperature increases during few hours, stabilizing after approximately 7 hours of exposure, which suggest a stabilization of the deposit after such time. This correlates well with the previous observations of the dynamic of LIC formation.

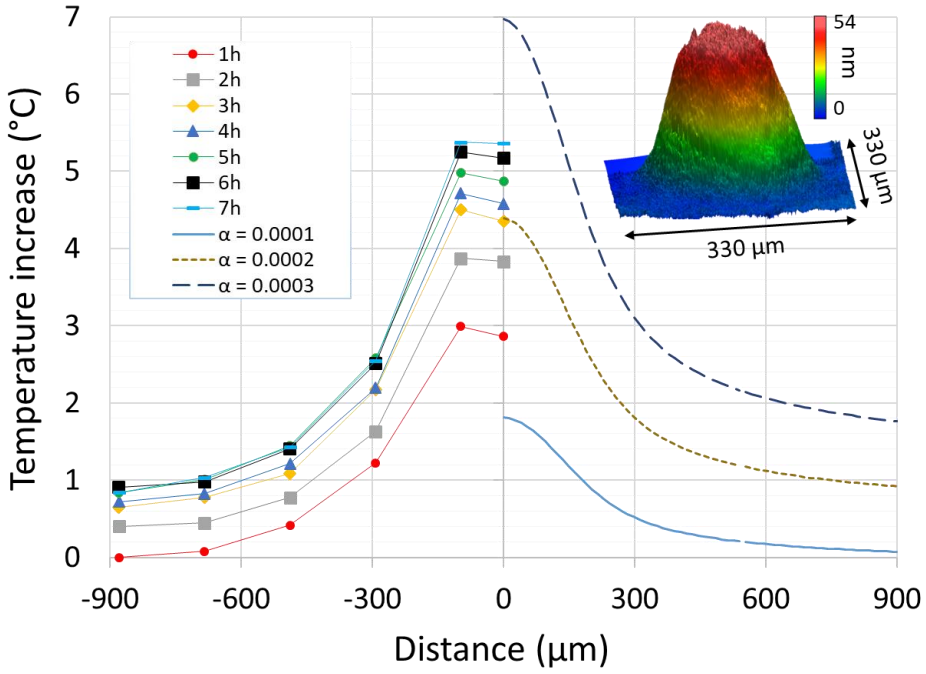

Figure 14: Temperature increase at the surface of a HR mirror exposed to 700 fs / 3.3 MHz pulses with a mean power of 35 W and a beam diameter of 550 µm. The beam is centred at 0 position. Left part of the figure: measurements at different time of the exposure; Right part of the figure: simulations of steady-state temperature for different absorption levels. Insert: Final deposit (after 7h of exposure) characterized by WLIM.

Even if not spatially resolved, these thermal measurements prove that the LIC formation is mainly a cold process (as opposed to pyrolysis process for instance), supporting the hypothesis of photo-activated polymerisation of contaminants on the surface of the optic.

In order to correlate these temperature measurements to the absorption level of the LIC deposit we have conducted thermal simulations. They were done with the Finite Element Software COMSOL Multiphysics, considering the sample geometry and a Gaussian surface heat source with lateral dimensions of the laser spot size. The sample was considered thermally isolated, conditions that are representative of the experiment (the sample is hold by 3contact points), with boundary conditions of surface radiation. The heat equation in conduction regime was solved to obtain the steady state temperature distribution, for different absorption levels of the incoming laser intensity. Results are shown on **Figure 14 f**or absorption levels of 200 to 400 ppm that give consistent temperature levels compared to the experiment. Such levels of absorption are also consistent with our measurements of drops of reflection of few percent (the remaining part of losses should be the contribution of scattering or interferential effects as suggested before). If we consider a 50 nm deposit, the estimated absorption level of deposited material corresponds to an extinction coefficient in the range 10^{-4} to $3x10^{-4}$. This corresponds to a weakly absorbing layer compared to pure carbon[49] and analysis of the deposit is required to understand its nature. At this point however we have not found a suitable technique for that purpose.

Conclusion

We have reported in this work on Laser Induced Contamination effects that can occur in the ultrashort regime at high repetition rate and high average power. This effect was shown to be detrimental for applications since the growth of a LIC deposit leads to absorption and scattering losses on the optics, at reduced fluences compared to laser damage occurrence. An experimental system has been developed to obtain reproducible LIC deposits through accelerated tests under well-controlled conditions, representative of laser operation on thousands of hours. This has enable an extensive study of LIC dynamics with different dedicated tools such as *in situ* microscopy,

White Light Interferometry and thermal imaging. Our analysis has led to the conclusion that dielectric mirrors submitted to 700 fs pulses at 515 nm with 3 MHz repetition rate in ambient air are contaminated by a few tens of nm deposit, possibly of carbon compounds, that continuously grow under the laser flux up to a saturation level (up to 100 nm). **Since previous works conducted on pulsed UV nanosecond have shown that LIC formation can be caused by UV activated polymerisation of contaminants on the surface of the optic, our hypothesis is that the same process occurs with green ultrashort pulses, but with two-photon polymerisation because of the high laser intensity.** The growth dynamic and saturation level is strongly dependent on the laser fluence, but also on the last layer of the dielectric stack (in air/film interface) which opens some perspective on the mitigation of this effect. The absorption level of the deposit (few hundreds of ppm from our estimations) leads to a local heat source on the surface and thermal gradients on the optics. It is however not clear at this point if the temperature increase assists or inhibits the contamination process.

Our study was conducted in ambient air but it is quite known from the state of the art (mainly in the field of space optics) that environmental conditions (humidity, oxygen concentration, organic materials in the system…) have dramatic impact on LIC effect. A following of this study could be conducted in order to identify the best operating conditions to minimize such contribution and improve reliability of laser components.

Acknowledgments

We thank Dr. Samira Khadir, who developed the monochromatic optical microscopy, for her help with the measurements on our samples, and Camille Petite for his help with thermal measurements.

References

1. Florent Thibault, “High Repetition Rate USP Lasers Improve OLED Cutting Results,” Coherent White Pap. (2018).
2. J. Choi et al., “Femtosecond Laser Based Manufacturing of Tailored Flexible Electronics for OLED and OPV Applications,” in Conference on Lasers and Electro-Optics, p. 929, Optical Society of America (2019) [doi:10.1364/CLEO_AT.2019.ATu4I.1].
3. D. Ristau, *Laser-Induced Damage in Optical Materials*, 1st ed., Detlev Ristau, Ed., CRC Press, Boca Raton, USA (2015).
4. E. G. Gamaly et al., “Ablation of solids by femtosecond lasers: Ablation mechanism and ablation thresholds for metals and dielectrics,” Phys. Plasmas **9**(3), 949–957 (2002) [doi:10.1063/1.1447555].
5. M. Mero et al., “Scaling laws of femtosecond laser pulse induced breakdown in oxide films,” Phys. Rev. B **71**(11), 115109, American Physical Society (2005) [doi:10.1103/PhysRevB.71.115109].
6. B. Mangote et al., “Femtosecond laser damage resistance of oxide and mixture oxide optical coatings,” Opt. Lett. **37**(9), 1478–1480, OSA (2012) [doi:10.1364/OL.37.001478].
7. M. Jupé et al., “Mixed oxide coatings for advanced fs-laser applications,” in Laser-Induced Damage in Optical Materials: 2007 **6720**, G. J. Exarhos et al., Eds., pp. 293–305, SPIE (2007) [doi:10.1117/12.753730].
8. A. Hervy et al., “Femtosecond laser-induced damage threshold of electron beam deposited dielectrics for 1-m class optics,” Opt. Eng. **56**(1), 1–8, SPIE (2016) [doi:10.1117/1.OE.56.1.011001].
9. M. Chorel et al., “Robust optimization of the laser induced damage threshold of dielectric

mirrors for high power lasers," Opt. Express **26**(9), 11764–11774, OSA (2018) [doi:10.1364/OE.26.011764].

10. M. Mero et al., "On the damage behavior of dielectric films when illuminated with multiple femtosecond laser pulses," Opt. Eng. **44**(5), 1–7, SPIE (2005) [doi:10.1117/1.1905343].
11. D.-B. Douti, L. Gallais, and M. Commandré, "Laser-induced damage of optical thin films submitted to 343, 515, and 1030 nm multiple subpicosecond pulses," Opt. Eng. **53**, 122509 (2014) [doi:10.1117/1.OE.53.12.122509].
12. S. M. Eaton et al., "Heat accumulation effects in femtosecond laser-written waveguides with variable repetition rate," Opt. Express **13**(12), 4708–4716, OSA (2005) [doi:10.1364/OPEX.13.004708].
13. B. J. Nagy et al., "Direct comparison of kilohertz- and megahertz-repetition-rate femtosecond damage threshold," Opt. Lett. **40**(11), 2525–2528, OSA (2015) [doi:10.1364/OL.40.002525].
14. M. Sozet et al., "Sub-picosecond laser damage growth on high reflective coatings for high power applications," Opt. Express **25**(21), 25767–25781, OSA (2017) [doi:10.1364/OE.25.025767].
15. R. A. Negres et al., "Laser-induced damage of intrinsic and extrinsic defects by picosecond pulses on multilayer dielectric coatings for petawatt-class lasers," Opt. Eng. **56**(1), 1–9, SPIE (2016) [doi:10.1117/1.OE.56.1.011008].
16. Y. Hao et al., "Asymmetrical damage growth of multilayer dielectric gratings induced by picosecond laser pulses," Opt. Express **26**(7), 8791–8804, OSA (2018) [doi:10.1364/OE.26.008791].

17. P. K. Velpula et al., “Evolution of femtosecond laser damage in a hafnia–silica multi-layer dielectric coating,” Opt. Lett. **44**(21), 5342–5345, OSA (2019) [doi:10.1364/OL.44.005342].

18. F. E. Hovis et al., “Mechanisms of contamination-induced optical damage in lasers,” in Laser-Induced Damage in Optical Materials: 1994 **2428**, H. E. Bennett et al., Eds., pp. 72–83, SPIE (1995) [doi:10.1117/12.213736].

19. H. A. Abdeldayem et al., “Contamination and radiation effects on spaceflight laser systems,” in Photonics for Space Environments X **5897**, E. W. Taylor, Ed., pp. 44–56, SPIE (2005) [doi:10.1117/12.622345].

20. M. Otto, “Airborne molecular contamination: quality criterion for laser and optical components,” in Components and Packaging for Laser Systems **9346**, A. L. Glebov and P. O. Leisher, Eds., pp. 88–97, SPIE (2015) [doi:10.1117/12.2076274].

21. D. Kokkinos et al., “Laser optics in space failure risk due to laser induced contamination,” CEAS Sp. J. **9** (2016).

22. G. G. El Reaidy et al., “Study of the first stages of laser-induced contamination,” Opt. Eng. **57**, 121903–121908 (2018).

23. C. T. Scurlock, “A phenomenological study of the effect of trace contamination on lifetime reduction and laser-induced damage for optics,” in Laser-Induced Damage in Optical Materials: 2004 **5647**, G. J. Exarhos et al., Eds., pp. 86–94, SPIE (2005) [doi:10.1117/12.601944].

24. P. Chen et al., “Contamination control of space-based laser instruments,” in Optical Systems Degradation, Contamination, and Stray Light: Effects, Measurements, and Control II **6291**, O. M. Uy, J. C. Fleming, and M. G. Dittman, Eds., pp. 35–46, SPIE

(2006) [doi:10.1117/12.681175].

25. U. Leinhos et al., “Long-term laser induced contamination tests of optical elements under vacuum at 351nm,” in Laser-Induced Damage in Optical Materials: 2010 **7842**, G. J. Exarhos et al., Eds., pp. 591–599, SPIE (2010) [doi:10.1117/12.869297].

26. W. Riede et al., “Laser-induced contamination on space optics,” in Laser-Induced Damage in Optical Materials: 2011 **8190**, G. J. Exarhos et al., Eds., pp. 331–344, SPIE (2011) [doi:10.1117/12.899190].

27. B. H. Weiller, J. D. Fowler, and R. M. Villahermosa, “Contamination resistant coatings for enhanced laser damage thresholds,” in Laser-Induced Damage in Optical Materials: 2012 **8530**, G. J. Exarhos et al., Eds., pp. 524–529, SPIE (2012) [doi:10.1117/12.2011179].

28. I. Balasa et al., “Enhancement of contamination growth and damage by absorption centers under UV irradiation,” in SPIE Laser Damage **9237**(1), p. 92372A (2014) [doi:10.1117/12.2085138].

29. H. Schröder et al., “Investigation of laser induced deposit formation under space conditions,” in International Conference on Space Optics — ICSO 2008 **10566**, J. Costeraste, E. Armandillo, and N. Karafolas, Eds., pp. 391–396, SPIE (2017) [doi:10.1117/12.2308207].

30. F. R. Wagner et al., “Laser induced deposits in contaminated vacuum environment: Optical properties and lateral growth,” Opt. Laser Technol. **122**, 105889 (2020) [doi:https://doi.org/10.1016/j.optlastec.2019.105889].

31. F. E. Hovis et al., “Contamination damage in pulsed 1-um lasers,” in 27th Annual Boulder Damage Symposium: Laser-Induced Damage in Optical Materials: 1995 **2714**, H. E.

Bennett et al., Eds., pp. 707–716, SPIE (1996) [doi:10.1117/12.240348].

32. O. Gilard et al., “Contamination induced optical damage in high power laser diodes,” Eur. Sp. Agency, Spec. Publ. (2006).

33. D. Kokkinos et al., “Real-time measurement of temperature variation during nanosecond pulsed-laser-induced contamination deposition,” Appl. Opt. **54**(36), 10579–10585, OSA (2015) [doi:10.1364/AO.54.010579].

34. H. Schröder et al., “Fluorescence monitoring of organic deposits,” in Laser-Induced Damage in Optical Materials: 2007 **6720**, G. J. Exarhos et al., Eds., pp. 233–241, SPIE (2007) [doi:10.1117/12.752866].

35. K. Bien-Aimé et al., “Impact of storage induced outgassing organic contamination on laser induced damage of silica optics at 351 nm,” Opt. Express **17**(21), 18703–18713, OSA (2009) [doi:10.1364/OE.17.018703].

36. O. Favrat et al., “Study of organic contamination induced by outgassing materials. Application to the Laser MégaJoule optics,” Appl. Surf. Sci. **293**, 132–137 (2014) [doi:https://doi.org/10.1016/j.apsusc.2013.12.116].

37. X. Cheng et al., “Surface Contaminant Control Technologies to Improve Laser Damage Resistance of Optics,” Adv. Condens. Matter Phys. **2014**, 1–7 (2014) [doi:10.1155/2014/974245].

38. E. S. Field and D. E. Kletecka, “Impact of contamination and aging effects on the long-term laser damage resistance of SiO2/HfO2/TiO2 high reflection coatings for 1054 nm,” Opt. Eng. **58**(10), 1–5, SPIE (2019) [doi:10.1117/1.OE.58.10.105105].

39. “ISO/TR 21254-4: Lasers and laser-related equipment - Test methods for laser-induced damage threshold - Part 4: Inspection, detection and measurement” (2011).

40. S. Khadir et al., “Optical imaging and characterization of graphene and other 2D materials using quantitative phase microscopy,” ACS Photonics, acsphotonics.7b00845 (2017) [doi:10.1021/acsphotonics.7b00845].

41. L. Yan et al., “Dual-wavelength investigation of laser-induced damage in multilayer mirrors at 532 and 1064nm,” Opt. Commun. **285**(12), 2889–2896 (2012) [doi:https://doi.org/10.1016/j.optcom.2012.02.028].

42. M. Mrohs et al., “Dual wavelength laser-induced damage threshold measurements of alumina/silica and hafnia/silica ultraviolet antireflective coatings,” Appl. Opt. **55**(1), 104–109, OSA (2016) [doi:10.1364/AO.55.000104].

43. D. E. Smith et al., “Mars Orbiter Laser Altimeter: Experiment summary after the first year of global mapping of Mars,” J. Geophys. Res. Planets **106**(E10), 23689–23722 (2001) [doi:10.1029/2000JE001364].

44. J. B. Abshire et al., “Geoscience Laser Altimeter System (GLAS) on the ICESat Mission: On-orbit measurement performance,” Geophys. Res. Lett. **32**(21) (2005) [doi:10.1029/2005GL024028].

45. P. Wagner, H. Schröder, and W. Riede, “In-situ laser-induced contamination monitoring using long-distance microscopy,” in Laser-Induced Damage in Optical Materials: 2014 **9237**, G. J. Exarhos et al., Eds., pp. 367–376, SPIE (2014) [doi:10.1117/12.2066465].

46. G. Gebrayel El Reaidy, “Evaluation expérimentale et modélisation de la contamination induite par laser sur les optiques spatiales,” Aix Marseille University (2018).

47. H. Schröder et al., “Investigation of UV laser induced depositions on optics under space conditions in presence of outgassing materials,” in International Conference on Space Optics — ICSO 2006 **10567**, E. Armandillo, J. Costeraste, and N. Karafolas, Eds., pp.

771–775, SPIE (2017) [doi:10.1117/12.2308066].

48. M. Ließmann et al., “Scaling of laser-induced contamination growth at 266nm and 355nm,” in Laser-Induced Damage in Optical Materials: 2015 **9632**, G. J. Exarhos et al., Eds., pp. 385–391, SPIE (2015) [doi:10.1117/12.2194083].

49. T. C. Bond and R. W. Bergstrom, “Light Absorption by Carbonaceous Particles: An Investigative Review,” Aerosol Sci. Technol. **40**(1), 27–67, Taylor & Francis (2006) [doi:10.1080/02786820500421521].

50. B. Wang and L. Gallais, “A theoretical investigation of the laser damage threshold of metal multi-dielectric mirrors for high power ultrashort applications,” Opt. Express **21**(12), 14698–14711, OSA (2013) [doi:10.1364/OE.21.014698].

List of Figures captions

Figure 1: A LIC deposit on a dielectric mirror exposed to 700 fs/ 515 nm/ 30 MHz laser with 35 W of mean power and 130 µm beam diameter (surface topography measured using White Light Interferometry).

Figure 2: The experimental configuration, described here for the tests of High-Reflectors with 45 degrees of incidence. The inserted image on the right is a close view of the sample area, with (1) the focusing lens, (2) the microscope, (3) the calorimeter and (4) the sample holder. These different elements are also numbered in the schematic. The inserted image on the left is a close view of one sample in the holder, with the microscope beneath it.

Figure 3: (a) Caustics of the focused laser beam by a plano-convex fused silica lens (f = 200 mm) measured via a beam profiler system (WinCamD-UHR). (b) Spatial beam profile when moving the focusing lens in different positions (All spatial beam profiles use similar scales).

Figure 4: Laser damage observed via (a) online microscopy and (b) Scanning Electron Microscopy on a HR mirror after 23 hours of laser exposure at 515 nm, 700 fs, 3.3 MHz, 35 W focused down to 86 µm diameter on the surface. Both figures use similar lateral scales.

Figure 5: *In situ* images showing the dynamics of LIC deposit formation on the surface of a HR mirror associated to transmission measurement. Test conditions: 72 hours of laser exposure at 515 nm, 700 fs, 3.3 MHz and 35 W focused down to 157 µm diameter on the surface.

Figure 6: (a) LIC deposit footprint (Same test shown in Figure 5) inspected via different *ex situ* diagnostics: (a) Optical Microscopy, (b) White Light Interferometry, (c) Transmittance and (d) Optical Path Difference (OPD) images for 590 nm wavelength light, (e) Confocal Microscopy (excitation at 488 nm). All figures (a-e) use similar scales.

Figure 7: (a) Results of the 515-nm irradiation on a dichroic mirror during 300 hours with d_{1/e^2} = 200 µm, 700 fs, 2 MHz and 28 W (b) Results of irradiation using the same dichroic mirror during 18 hours with d_{1/e^2} = 210 µm, 700 fs, 3.3 MHz and 35 W.

Figure 8: Two different tests performed on a sample under the same conditions. LIC deposits were inspected after each run (WLIM). Test conditions: 72 hours of laser exposure at 515 nm, 700 fs, 3.3 MHz and 35 W focused down to 157 µm diameter on the surface.

Figure 9: Variation of LIC deposit thickness measured via WLIM, after 2 hours of laser exposure (700 fs, 3.3 MHz, 35 W) with spot sizes in the range 87-210 µm (diameter at $1/e^2$).

Figure 10: Dynamic of deposit formation on the surface of a HR mirror. Test conditions: 18 hours of laser exposure at 515 nm, 700 fs, 3.3 MHz and 35 W focused down to 210 µm diameter on the surface.

Figure 11: Dynamic of deposit formation. The deposit height was measured via WLIM. The test was performed at a wavelength of 515 nm, a pulse duration of 700 fs, a repetition rate 3.3 MHz and 35 W focused down to 133 µm diameter on the surface.

Figure 12: (a) *Ex situ* WLIM of the irradiated site. Relative transmission of the LIC deposit using different monochromatic sources at (b) 530 nm, (c) 590 nm and (d) 625 nm. Test conditions: 72 hours of laser exposure at 515 nm, 700 fs, 3.3 MHz and 35 W focused down to 157 µm diameter on the surface.

Figure 13: Comparison between LIC deposits area measured via WLIM, after 2 hours of laser exposure (700 fs, 3.3 MHz, 35 W) and the beam area at different spot sizes.

Figure 14: Temperature increase at the surface of a HR mirror exposed to 700 fs / 3.3 MHz pulses with a mean power of 35 W and a beam diameter of 550 µm. The beam is centred at 0 position. Left part of the figure: measurements at different time of the exposure; Right part of the figure: simulations of steady-state temperature for different absorption levels. Insert: Final deposit (after 7h of exposure) characterized by WLIM.